



INTERNATIONAL
JOURNAL OF
SEDIMENT
RESEARCH
www.elsevier.com/locate/ijsrc

International Journal of Sediment Research 29 (2014) 414-422

# Experimental study of debris flow caused by domino failures of landslide dams

Hua-Yong CHEN<sup>1</sup>, Peng CUI<sup>2\*</sup>, Gordon G. D. ZHOU<sup>3</sup>, Xing-Hua ZHU<sup>4</sup>, and Jin-Bo TANG<sup>5</sup>

#### Abstract

The formation of landslide dams is often induced by earthquakes in mountainous areas. The failure of a landslide dam typically results in catastrophic flash floods or debris flows downstream. Significant attention has been given to the processes and mechanisms involved in the failure of individual landslide dams. However, the processes leading to domino failures of multiple landslide dams remain unclear. In this study, experimental tests were carried out to investigate the domino failure of landslide dams and the consequent enlargement of downstream debris flows. Different blockage conditions were considered, including complete blockage, partial blockage and erodible bed (no blockage). The mean velocity of the flow front was estimated by videos. Total stress transducers (TSTs) and Laser range finders (LRFs) were employed to measure the total stress and the depth of the flow front, respectively. Under a complete blockage pattern, a portion of the debris flow was trapped in front of each retained landslide dam before the latter collapsed completely. This was accompanied by a dramatic decrease in the mean velocity of the flow front. Conversely, under both partial blockage and erodible bed conditions, the mean velocity of the flow front increased gradually downward along the sloping channel. Domino failures of the landslide dams were triggered when a series of dams (complete blockage and partial blockage) were distributed along the flume. However, not all of these domino failures led to enlarged debris flows. The modes of dam failures have significant impacts on the enlargement of debris flows. Therefore, further research is necessary to understand the mechanisms of domino failures of landslide dams and their effects on the enlargement of debris flows.

Key Words: Debris flow, Landslide dams, Domino failures, Enlargement of debris flow, Mean velocity

# 1 Introduction

Heavy rainfalls often trigger flash floods, debris flows, structural collapses and/or landslides, resulting in loss of life as well as damage to public and private properties. This is particularly problematic in mountainous areas in China. On August 8, 2010, a very large debris flow occurred in the Sanyanyu and Luojiayu gullies, north of ZhouQu county, Gansu province, resulting in significant loss of farmlands and destruction of several villages. The debris flow then blocked the Bailongjiang River, resulting in the formation of a lake that inundated over half of ZhouQu. Altogether, this event resulted in 1,248 deaths, and 496 were declared missing (Hu et al., 2010). Field observations revealed that large amounts of landslide dams composed of granular materials were found along the gullies. Domino failures of landslide dams in such gullies are considered to be one of the primary reasons for the enlargement of debris flows.

The failure of conventional or landslide dams has been investigated extensively in recent years. Such studies have been based on theoretical solutions, physical modeling, or numerical simulations. For example, Hunt (1982, 1987) analyzed finite-length reservoirs to generate equations to calculate the threshold dam-break flow in terms of upstream and downstream water depths. Wu and Wu (1988) and Wu et al. (1996) developed a new theoretical method to calculate the hydraulic characteristics of the dam-break flow with arbitrary outlets. Next, they provided a computational method

<sup>&</sup>lt;sup>1</sup> Asst. Prof., Key Laboratory of Mountain Hazards and Earth Surface Process, CAS, Chengdu 610041, China, Institute of Mountain Hazards and Environment, CAS, Chengdu 610041, China. E-mail: hychen@imde.ac.cn.

<sup>&</sup>lt;sup>2</sup> Prof., Key Laboratory of Mountain Hazards and Earth Surface Process, CAS, Chengdu 610041, China, Institute of Mountain Hazards and Environment, CAS, Chengdu 610041, China.

<sup>\*</sup> Corresponding author, E-mail: pengcui@imde.ac.cn. Tel: 86-28-85214421.

<sup>&</sup>lt;sup>3</sup> Asso. Prof., Key Laboratory of Mountain Hazards and Earth Surface Process, CAS, Chengdu 610041, China, Institute of Mountain Hazards and Environment, CAS, Chengdu 610041, China. E-mail: gordon@imde.ac.cn.

<sup>&</sup>lt;sup>4</sup> Ph. D. candidate, Key Laboratory of Mountain Hazards and Earth Surface Process, CAS, Chengdu 610041, China, Institute of Mountain Hazards and Environment, CAS, Chengdu 610041, China. E-mail: zhuxinghua09@163.com.

<sup>&</sup>lt;sup>5</sup> Research Asst., Key Laboratory of Mountain Hazards and Earth Surface Process, CAS, Chengdu 610041, China, Institute of Mountain Hazards and Environment, CAS, Chengdu 610041, China. E-mail: jinbotang@imde.ac.cn.

Note: The original manuscript of this paper was received in Aug. 2012. The revised version was received in Jan. 2014. Discussion open until Sept. 2015.

which was applicable to describe a dimensionless hydrograph of the dam-break flow. Soares-Frazão (2007) studied the propagation of the dam-break flow in a channel with a triangular bottom, using two different measurement techniques: water level gauges and high speed digital cameras. In addition, an automated procedure was designed to measure the water depth based on the digital images. All of the aforementioned studies were based on the assumption that the dams in question collapsed instantaneously. However, in many cases, these dams (moraine dams, landslide dams, etc.) collapsed gradually because of the hydrodynamics of the water flow. Balmforth et al. (2008) carried out an experimental and theoretical study on displacement waves and discovered that a single wave was generally insufficient to collapse a dam; however, the seiche created by a large disturbance could breach the dam at a nearly full reservoir. In this situation, the wave could lead to a catastrophic erosional incision of a moraine dam. Cui et al. (2003) studied the conditions accompanying changes in the motion of debris flows caused by glacial lake outburst floods (GLOF). Their study revealed that the slope of the channel played a crucial role in the debris flow initiation and motion processes. Additionally, six patterns were identified with respect to modeling the relationship between the GLOF and subsequent debris flows. On this basis, measures for the mitigation of debris flow hazards were suggested. An experimental study of the inundation and landslides induced by dam-break floods over erodible beds in open channels was also carried out (Yan and Cao, 2009). Additionally, empirical formulas for predicting dam failures were proposed to calculate flood or debris flow discharges (Cheng et al., 2007; Chen et al., 2004). Numerical models were also employed to simulate the hydraulic characteristics of the flood flow downstream (Wang et al., 2008; Yue et al., 2007; Cao et al., 2011a). Dam-break flows may change into debris flow if certain basic conditions are satisfied, such as abundant loose material sources, a river bed with steep slope, etc. (Li et al., 2011; Hu et al., 2011). However, few studies have investigated domino failures of landslide dams and enlargement of debris flows (Cao et al., 2011b), which is the focus of this study.

For each experimental test, video cameras were used to record the complete evolutionary process of the debris flow. The mean velocity of the flow front was estimated by recording the movement of the flow front along the flume. The total stress and depth of the debris flow were measured in different cross-sections under both partial blockage and erodible bed patterns. In addition, the enlargement of debris flows under these different patterns was analyzed.

## 2 Design of simulation experiments

### 2.1 Experimental flume

Field investigations indicated that domino failures of landslide dams and enlargement of debris flows had occurred in the Sanyanyu and Luojiayu gullies. Therefore, we conducted an extensive simulation to study the dynamics of a gravity-driven debris flow. The experimental flume consisted of an upstream reservoir, a sluice gate, and a downstream channel. The upstream reservoir was 4.60 m long, 0.7 m wide and 1.4 m high, with a horizontal bottom. The downstream channel was 47.3 m long, 0.7 m wide and 1.4 m high, with a slope of 12°. The sluice gate was used to control the water depth of the upstream reservoir. The sudden upward detachment of the gate was regarded as an instantaneous complete failure of the upstream dam. Five transparent rectangular glass panels, (each 1.2 m wide by 1.5 m long) were placed at regular intervals to observe the process of landslide dam collapses and to estimate the depth of debris flows. Laser range finders (LRFs) were used to obtain the time evolution of the depth of the debris flow at C1 and C3. Total stress transducers (TSTs) were employed to obtain the time evolution of the total stress (expressed in mV) at three cross-sections (C1, C2, and C3) (Fig. 1).

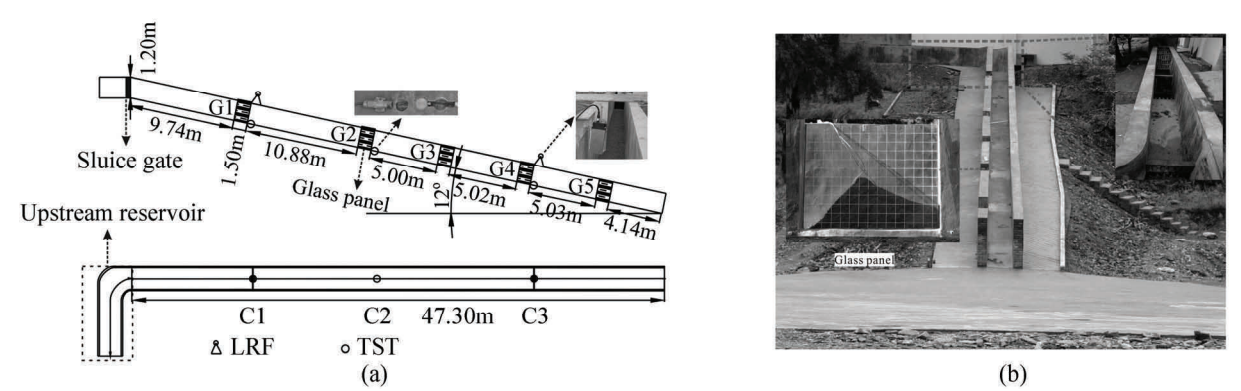


Fig. 1 Experimental setup: (a) schematic diagram of the experimental setup; (b) photographs of the experimental setup

# 2.2 Instrument installation and measurement

The use of video cameras for estimating debris flow depths is not always reliable, particularly when such flows travel along an irregular river bed at a relatively high speed. The depth of debris flows can be measured directly by LRFs. Their measurement range was up to 30.0 m with an accuracy of  $\pm 0.001$  m. The sampling frequency was 31.0 Hz.

TSTs are capable of converting pressure signals into analog and then digital signals, which can then be identified and analyzed by a computer. Their measurement range was 0–200.0 kPa and the corresponding voltage  $V_t$  was set over a range of 0–5,000 mV. The transducers provided an accuracy of  $\pm 0.01$  mV and their sampling frequency was 25.0 Hz. The total stress ( $P_t$ ) is directly proportional to the voltage,  $V_t$ .  $P_t$  can be described as:

$$P_{t} = \frac{200}{5000} V_{t} = 0.04 (kPa / mV) \times V_{t}(mV)$$
 (1)

where  $P_t$  is the total stress, and  $V_t$  is the voltage measured by TSTs.

Despite their drawbacks, video recordings of flow patterns remain one of the most important observation tools for debris flows. In our experiments, a video camera was installed at the downstream end of the flume to record the propagation of the debris flow in the flume. The mean velocity of the flow front was estimated based on the duration it took for the flow front to cover a certain distance as observed by video.

## 2.3 Experimental design and general patterns of landslide dams

A key question is how domino failures of landslide dams amplify debris flows in gullies. In the study area, the basic geometric features of the landslide dams, the distribution of the landslide dams and the slopes of the gullies were obtained through field investigations. In this study, various landslide dam patterns were set in the flume to study the process of the landslide dam failure and enlargement of the debris flow.

Three patterns of the granular material behavior were considered to investigate the propagation of debris flows, namely, complete blockage, partial blockage, and erodible bed (no blockage). Under the complete blockage pattern, three identical landslide dams ( $D_{F1}$ ,  $D_{F2}$  and  $D_{F3}$ ) were erected at the locations where the glass panels  $G_1$ - $G_3$  were present such that the erosion process of each dam could be observed. Another dam ( $D_{F0}$ ) was placed between the sluice gate and the first landslide dam ( $D_{F1}$ ) to provide solid granular material for the dam-break flood. Each landslide dam was 1.5 m in length and 0.6 m in height, with a width equal to that of the flume (Fig. 2(a)). Under the partial blockage pattern, instead of a dam like  $D_{F0}$ , an erodible bed was placed between the sluice gate and the first landslide dam ( $D_{P1}$ ) to provide the granular material for floods. This bed was 19.2 m in length and 0.05 m in height. The three identical landslide dams ( $D_{P1}$ ,  $D_{P2}$  and  $D_{P3}$ ) possessed semi-elliptical cone shapes, each 2.9 m in diameter and 0.5m in height (Fig. 2(b)). Under the erodible bed pattern, the entire channel (47.3 m long) was covered with a layer of granular material (0.05 m thick) (Fig. 2(c)). For all blockage patterns, the granular material was composed of fine particles with diameters smaller than 0.02 m. The basic parameters of the upstream reservoir and the granular material are shown in Table 1.

### 3 Experimental results and analysis

### 3.1 Debris flow pattern and velocity variation

Under the complete blockage pattern (Fig. 3a. (1)), the dam-break flow rose upwards along the upstream face of  $D_{F0}$  and then traveled downstream as opposed to being trapped behind the landslide dam. Erosion occurred on the surface of  $D_{F0}$  and significant amount of granular material was eroded away by the dam-break flow, leading to the formation of a debris flow. This continued moving towards  $D_{F1}$ , but the mean velocity of the flow front decreased gradually due to its relatively high viscosity. Therefore, a portion of the debris flow was trapped in front of  $D_{F1}$  and a reservoir formed behind the landslide dam. The interaction between the trapped debris flow and the moving debris flow enhanced the energy dissipation due to mixing and the turbulence. Both the discharge and velocity of the debris flow decreased as it passed over  $D_{F1}$ . In other words, the evolution of the debris flow could be considered as a process of energy dissipation. After the flow front passed over  $D_{F1}$ , it continued to travel towards the next landslide dam. The velocity of the first flow front of the debris flow was too low to pass over  $D_{F2}$ , and therefore, the flow front was trapped behind  $D_{F2}$ . When the volume of the debris flow behind  $D_{F2}$  exceeded certain threshold value, the stepped debris flow was able to pass over the landslide dam and travel to the next dam (Fig. 3a. (2)–(4)). During the entire process of the debris flow propagation, intermittent debris flows and domino failures of landslide dams occurred when the debris flow passed over each corresponding landslide dam. In addition, the erosion of the landslide dams did not stop until the flow reached the bottom of each dam (Fig. 3a. (5)).

Under the partial blockage pattern, the dam-break flow propagated over the erodible bed before it arrived at the first landslide dam,  $D_{P1}$  (Fig. 3b. (1)). The energy dissipation of the debris flow was enhanced due to the roughness of the erodible bed. Therefore, the mean velocity of the first flow front at a distance of 11.0 m (from  $D_{P1}$ ) was lower than that of the corresponding flow front under the complete blockage pattern (Fig. 4). Different from the debris flow under the complete-blockage pattern which was trapped before the landslide dam collapsed, the debris flow under the partial-blockage pattern moved down easily from the lower elevation of each dam and took a significant amount of granular material away from the landslide dam. This resulted in domino failures of all the landslide dams and the enlargement of the debris flow (Fig. 3b. (2)–(5)). The mean velocity of the flow front increased gradually along the channel.

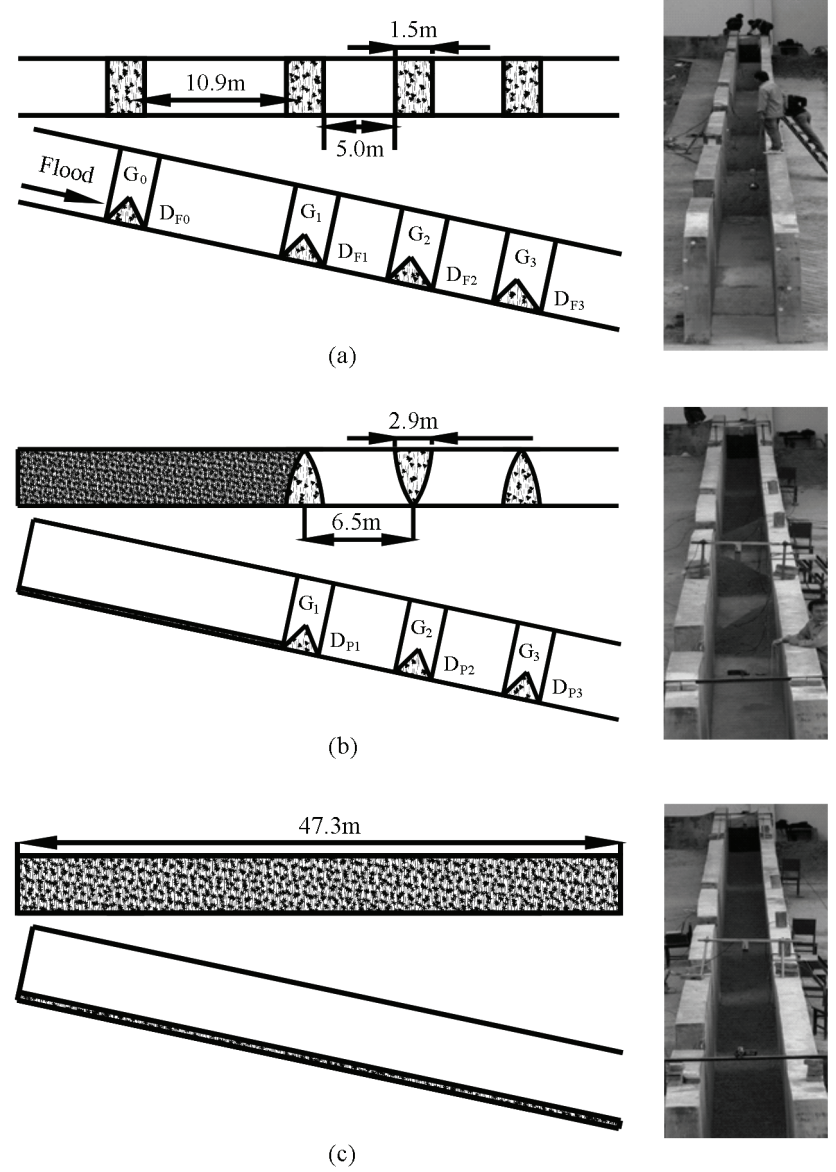


Fig. 2 Layouts of the three artificial blockage patterns in the flume: (a) for the complete blockage pattern, four landslide dams were placed to the right of the glass panels; (b) for the partial blockage pattern, an erodible bed and three partial landslide dams were placed along the flume; (c) for the no-blockage pattern, an erodible bed was placed along the flume.

Table 1 Basic parameters of the upstream reservoir and granular material under different blockage patterns

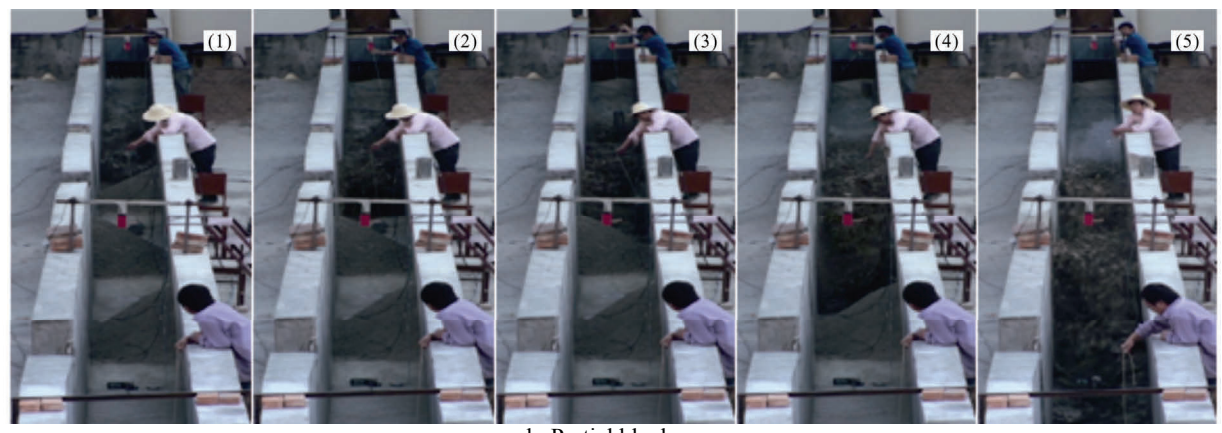
Patterns	Upstream reservoir		Granular material	
	Water depth (m)	Volume (m <sup>3</sup> )	Volume (m <sup>3</sup> )	Void ratio
Complete blockage	0.45	1.45	1.41	0.4
Partial blockage	0.56	1.80	2.70	0.4
Erodible bed	0.56	1.80	2.40	0.4

Under the erodible bed pattern, the debris flow moved easily through the channel, since the component of gravity along the inclined granular bed was more than sufficient to compensate for the frictional resistance created by the granular material. Therefore, the mean velocity of the debris flow increased gradually, and increasingly greater amounts of granular materials became entrained by the debris flow as it traveled along the flume (Fig. 3c).

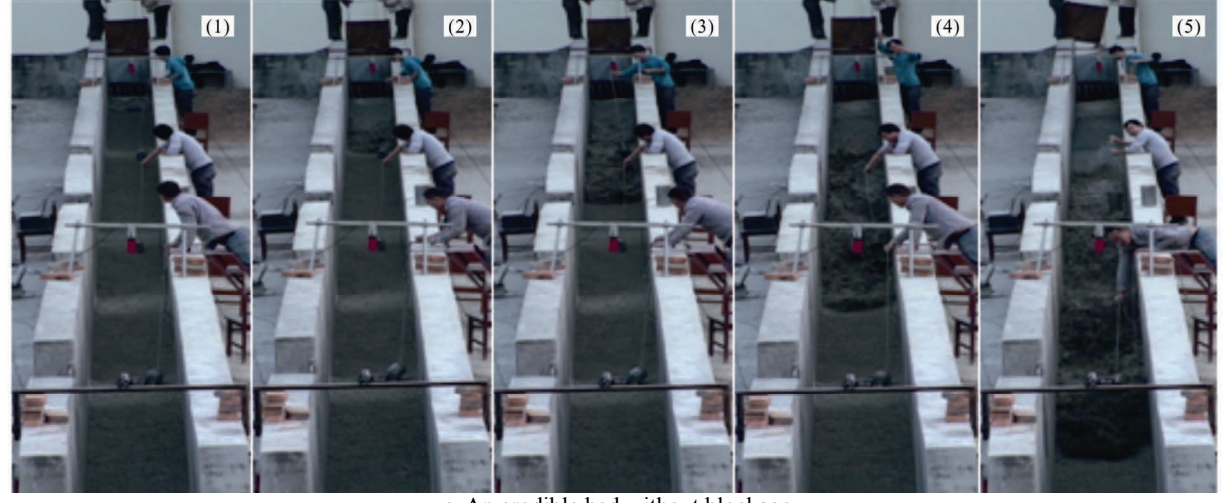
Under the complete blockage pattern, the landslide dams evidently had a significant impact on the debris flow. The mean velocity of the debris flow front decreased dramatically as it transcended the series of the landslide dams. However, the mean velocity of the debris flow front increased when a flow channel was provided in the partial blockage and erodible bed patterns (Fig. 4).



a. Complete blockage



b. Partial blockage



c. An erodible bed without blockage

Variation in debris flow patterns under different conditions: a. variation in debris flow patterns under complete blockage; b. variation in debris flow patterns under partial blockage; c. variation in debris flow patterns in the presence of an erodible bed without blockage.

# 3.2 Total stress and depth of the debris flow

The total stress  $P_t$  exerted on the flume bed by the debris flow comprised effective stress and pore pressure. It was directly affected by the depth of the debris flow front, as measured by the laser range finders. The bottom of the flume was considered to be the reference plane linking C1 and C3, respectively. Accordingly,  $P_t$  could be expressed as follows:

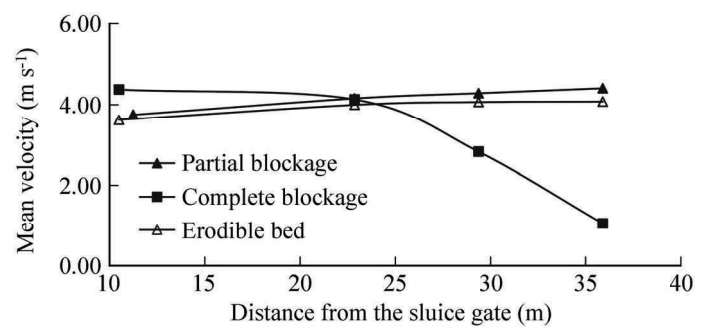


Fig. 4 Variation in mean flow front velocity along the flume

$$P_t = \rho_d g(h_s - h_c) \tag{2}$$

$$h_d = h_s - h_c \tag{3}$$

Here,  $\rho_d$  can be described as:

$$\rho_d = \frac{P_t}{h_d g} \tag{4}$$

where  $\rho_d$  is the density of the flow front, g is the acceleration due to gravity, and  $h_s$  is the distance between the debris flow surface and the reference plane. Similarly,  $h_c$  is the distance between the initial granular material surface and the reference plane before the debris flow front arrived at either C1 or C3. Finally,  $h_d$  is the depth of the debris flow

Under the complete blockage pattern, the debris flow passed over D<sub>F1</sub> at a relatively high speed (about 4.4 m s<sup>-1</sup>) and then descended onto the bed. Data obtained by the LRF or TST appeared to be inaccurate due to the strong fluctuations observed in the debris flow movement. Hydraulic parameters under this pattern were not considered.

Under the partial blockage pattern, only the effective stress of granular material on the erodible bed was exerted on the transducers before the debris flow arrived at C1. The total stress increased rapidly as the flow fronts reached C1 and then decreased gradually because a significant amount of granular material was entrained by the debris flow. The total stress at C3 followed a trend similar to that at C1 and its peak value was about 2.5 times as large as that at C1 (Fig. 5a). In order to measure the depth of the debris flow in the designated cross-sections, two LRFs were deployed at C1 and C3, respectively. The initial depth,  $h_c$ , of the granular material was about 0.05m before the debris flow arrived at C1; increased dramatically when the flow front reached C1; and then quickly decreased to zero. However, a transparent dam-break flood was observed to propagate at C1. The LRF laser was able to easily penetrate the transparent flow to reach the bottom of the flume. At C3 (fixed flume bed),  $h_c$  was equal to 0.0m because no granular material was present. In other words, the depth of the debris flow  $h_d$  was equal to  $h_s$ . Unlike the variation in  $h_s$  at C1,  $h_s$  attained its maximum value and then decreased gradually, because the discharge of the debris flow decreased after the flow front arrived at C3. The maximum value of  $h_s$  was twice as high as that at C1 (Fig. 5b).

Under the erodible bed pattern, the evolution of the total stress and the depth of the debris flow followed the same trend as that under the partial blockage pattern at both C1 and C3. However, corresponding dynamic parameters at C3 were only 1.7 and 1.6 times as large as those at C1 as shown in Fig. 6.

As indicated in Table 2, the predicted results were in good agreement with the experimental data under both partial blockage and erodible bed patterns. The minimum and maximum absolute error was 3.85% and 5.47%, respectively. The reason why the discrepancy existed between the predicted and experimental data was as follows: Firstly, instrument errors were encountered when the flow depth was measured using LRFs. Debris flows were typically unsteady. The flow front was observed to fluctuate dramatically along the flume. The laser beam tended to be reflected by the surging flow front, which could decrease the accuracy and precision of the depth measurements. Secondly, human errors with respect to sampling and measurements of the debris flow likely have resulted in decreased precision.

### 3.3 Enlargement of debris flow along the flume

The velocity and depth are the most important hydrodynamic parameters reflecting the enlargement of debris flows. Under the complete blockage pattern, erosion began to occur at the top of each landslide dam, and the debris flow was trapped behind the remaining structure of the dam. This also resulted in a decrease of the flow front velocity along the flume. No enlargement of the debris flow was observed under this pattern, except when the landslide dams collapsed rapidly (whether partially or completely). Under the partial blockage and erodible bed patterns, the velocity of the debris flow at different cross-sections along the flume was measured (Fig. 4). However, the LRFs measured the depths of the debris flow only at C1 and C3. In order to obtain the variation of the debris flow discharges along the sloping

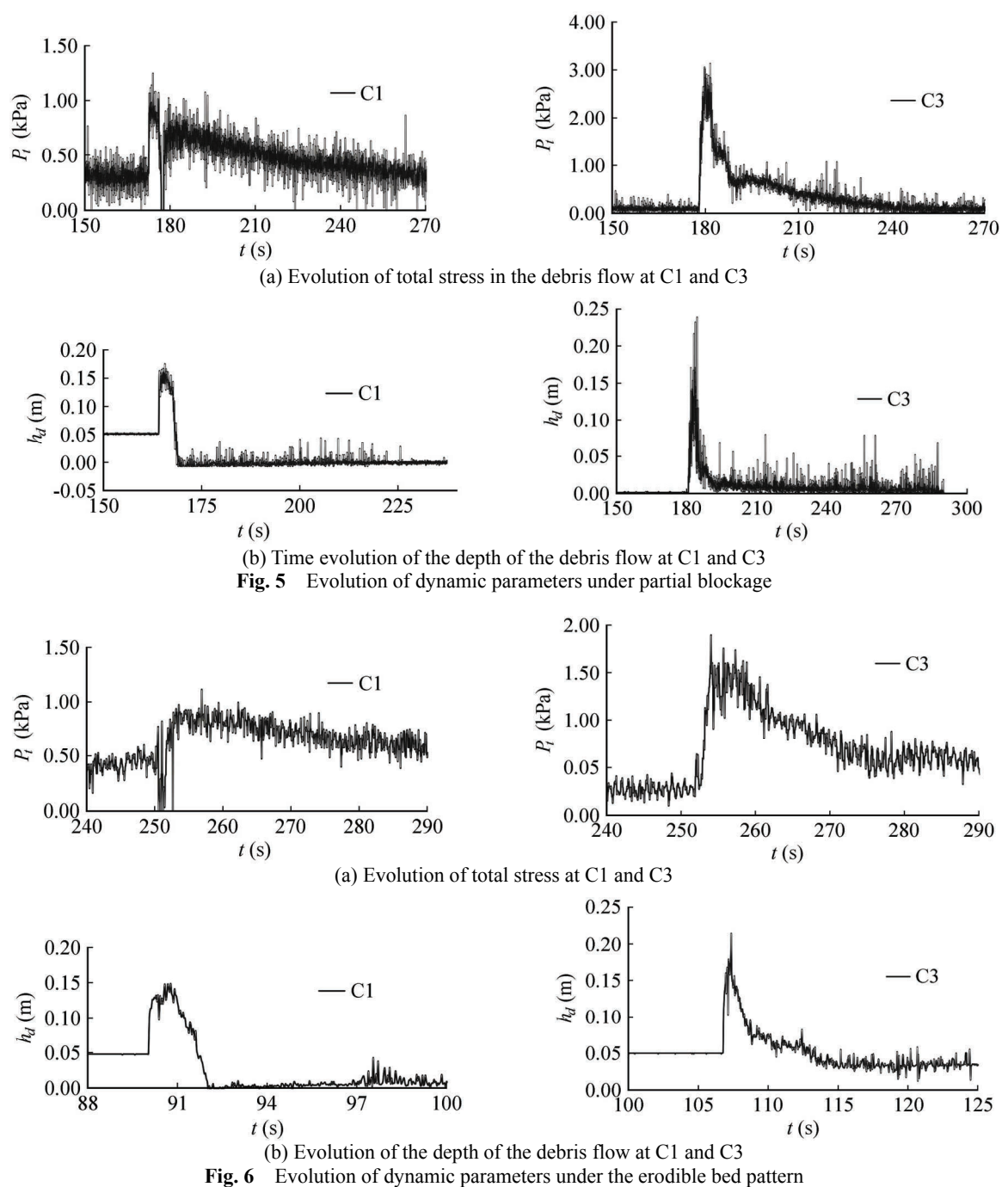


**Table 2** Comparison of experimental and theoretical values of  $\rho_d$  under different blockage patterns

Patterns	Cross-section	Density of flow front $\rho_d$ (g cm <sup>-3</sup> )		Error (%)
		Experimental	Theoretical	E1101 (70)
Partial blockage	C1	1.08	1.04	3.85
	C3	1.21	1.28	-5.47
Erodible bed	C1	1.20	1.14	5.26
	C3	1.27	1.21	4.96

channel, the change in the depth between C1 and C3 was analyzed. As indicated in Table 2, the density of the flow front, determined using Eq. (4), was in good agreement with the experimental observations. Thus, it is reasonable to use Eq. (4) to describe the relationship between the total stress and the density and depth of the debris flow. Equation (4) can also be written as:

$$h_d = \frac{P_t}{\rho_d g} \tag{5}$$

The parameters in Eq. (5) have the same definitions as the ones in Eq. (4). Therefore, the debris flow depth  $h_d$  at C2 was estimated using Eq. (5), provided that the values of  $P_t$  and  $\rho_d$  were obtained experimentally as shown in Table 3.

**Table 3** Estimation of  $h_d$  under partial blockage and erodible bed patterns

Patterns	Cross-section	$P_t$ (kPa)	$ ho_d$ (g cm <sup>-3</sup> )	$h_d$ (m)
Partial blockage	C2	2.49	1.28	0.20
Erodible bed	C2	1.74	1.61	0.11

The depth of the debris flow at Ci (i=1, 2, or 3) along the flume is shown in Fig. 7(a). The depth of the debris flow increased along the flume under both the partial blockage and erodible bed patterns. Furthermore, the depth of the debris flow was greater under the former pattern than that under the latter. Therefore, it was concluded that the peak discharge increased as the debris flow travelled downstream along the flume (Fig. 7(b)). Therefore, enlargement of the debris flow along the flume existed under both of these patterns, which could be described by the coefficient of peak discharge amplification  $\eta$ , as follows:

$$\eta = \frac{Q_{C3}}{Q_{C1}} \tag{6}$$

where  $\eta$  is the coefficient of peak discharge amplification, and  $Q_{C3}$  and  $Q_{C1}$  are the peak discharge of the flow front at C3 and C1, respectively.

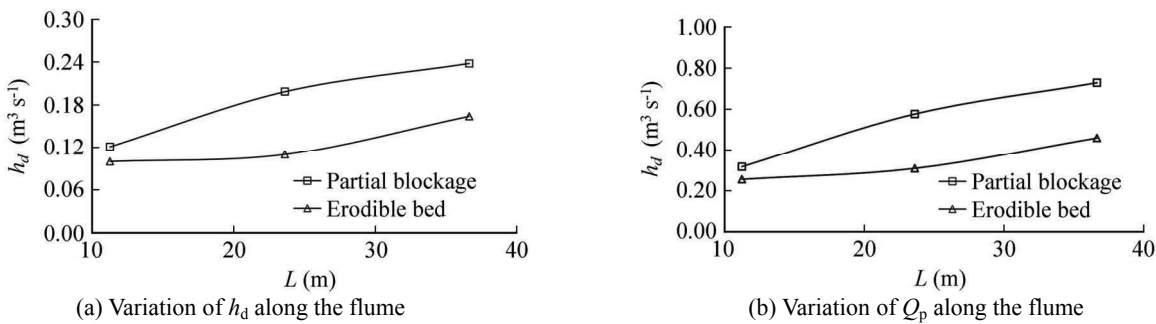


Fig. 7 Variation in  $h_d$  and  $Q_p$  along the flume under the partial blockage and erodible bed patterns

The enlargement effect under the partial blockage pattern was more obvious than that under the erodible bed pattern. This was because of the occurrence of the domino failure of the artificial landslide dams. The coefficient of peak discharge amplification,  $\eta$ , under the partial blockage and erodible bed patterns was 3.3 and 2.1, respectively. The primary reason for this variation was that, under the former pattern, the instantaneous velocity of the debris flow increased due to a sudden contraction of the cross-section when the flow front transited each landslide dam and a large amount of the granular material from these dams were transported at high speeds. Under the erodible bed pattern, erosion occurred on the surface of the granular material, creating greater frictional resistance than the smooth and rigid bed along the flume. Therefore the amount of granular material transported by the debris flow was less than that under the partial blockage pattern.

## 3.4 Discussion

In this study, domino failures of landslide dams occurred under both complete and partial blockage patterns. However, the enlargement of the debris flow occurred only under the partial blockage pattern. Under complete blockage, the mean velocity and peak discharge of the flow front decreased along the flume. This might be a result of the interaction between the trapped debris flow and stepped debris flow, which enhanced the energy dissipation. Under such conditions, the artificial landslide dams collapsed due to the flow front flowing over the tops of the dams, leading to the formation of intermittent debris flows. The major limitation of this experiment was that the process of dam failure was triggered by a relatively small simulated flash flood upstream. However the potential for a rapid sequential failure of landslide dams following a large flood discharge was not considered. When the flash flood is large enough to quickly destroy the landslide dams, the collapse model must be adjusted accordingly. Therefore, certain issues such as the mechanism of the domino failure of landslide dams, the dam failure processes, and the enlargement of debris flows will require elucidation in future studies.

#### 4 Conclusions

Based on the different conditions of the blockages, the dynamic process of the debris flow was investigated in a large-scale flume. The enlargement of debris flows under these different patterns was analyzed by studying the variation in related hydraulic parameters. The following conclusions were drawn based on this study:

- 1. The flow pattern and mean velocity of the flow front was dramatically different between the different patterns. Under the complete blockage pattern, the flow front was gradually trapped by the landslide dams. The interaction between the trapped debris flow and stepped debris flow enhanced the energy dissipation. The mean velocity of the debris flow decreased dramatically along the flume. Intermittent debris flow occurred when the debris flow front was trapped and then traveled over the dams. On the contrary, the debris flow traveled downstream easily and their mean velocities increased gradually under both the partial blockage and erodible bed patterns. Domino failures of landslide dams (complete as well as partial blockage) occurred when the dams were distributed along the flume.
- 2. With respect to the density of the flow front samples, the discrepancy between the theoretical and experimental values remained below 5.5% (absolute error). Therefore, the formula used to describe the relationship between the total stress and the density and depth of the debris flow is realistic.
- 3. Although domino failures of landslide dams occurred under the complete blockage pattern, the mean velocity and peak discharge of the flow front decreased due to the strong blocking effects. Very little enlargement of the debris flow was observed under this pattern. In contrast, significant debris flow enlargement was observed under the partial blockage and erodible bed patterns. The coefficient of peak discharge amplification  $\eta$  was 3.3 and 2.1, respectively.

### Acknowledgements

This study was supported by the Key Program of the National Natural Science Foundation of China (Grant No. 41030742), the Key Research Program of the Chinese Academy of Sciences (Grant No. KZZD-EW-05-01), the Youth Foundation of the Institute of Mountain Hazards and Environment, CAS (Grant No. SDS-QN-1302), and Youth Foundation of Key Laboratory of Mountain Hazards and Earth Surface Process, CAS.

#### References

Balmforth N. J., Von Hardenberg J., Provenzale A., and Zammett R. 2008, Dam breaking by wave-induced erosional incision. Journal of Geophysical Research, Vol. 113, pp. 1–12.

Cao Z. X., Yue Z. Y., and Pender G. 2011, Flood hydraulics due to cascade landslide dam failure. Journal of Flood Risk Management, No. 4, pp. 104–114.

Cao Z. X., Yue Z. Y., and Pender G. 2011, Landslide dam failure and flood hydraulics. Part II: Coupled mathematical modeling. Nat Hazards, No. 59, pp. 1021–1045.

Chen X. Q., Chen N. S., and Cui P. 2004, Calculation of discharge of debris flow induced by glacier lake outburst. Journal of Glaciology and Geocryology, Vol. 26, No. 3, pp. 357–362 (in Chinese).

Cheng Z. L., Geng X. Y., Dang C., and Liu J. J. 2007, Modeling experiment of break of debris-flow dam. Wuhan university Journal of Natural Sciences, Vol. 12, No. 4, pp. 588–594.

Cui P., Ma D. T., Chen N. S., and Jiang Z. X. 2003, The initiation, motion and mitigation of debris flow caused by glacial lake outburst. Quaternary Sciences, Vol. 23, No. 6, pp. 621–628 (in Chinese).

Hu K. H., Ge Y. G., Cui P., Guo X. J., and Yang W. 2010, Preliminary analysis of extra-large -scale debris flow disaster in Zhouqu County of Gansu Province. Journal of Mounta In Science, Vol. 28, No. 5, pp. 628–634 (in Chinese).

Hu X. D., Bi Y. H., and Wei J. 2011, Conditions leading to the destructive debris flow at the Sanyanyu Gulley and its occurrence trend. The Chinese Journal of Geological Hazard and Control, Vol. 22, No. 2, pp. 55–60 (in Chinese).

Hunt B.1982, Asymptotic solution for dam-break problem. Journal of the Hydraulics Division., ASCE, Vol. 109, No. 12, pp. 1698–1706.

Hunt B. 1987, A perturbation solution of the flood-routing problem. Journal of Hydraulic Research, Vol. 25, No. 2,pp. 215-234.

Li R. D., Wang G. L., Zhao C., Hu X. D., Zhu L. F., and Zeng Q. M. 2011, Analysis of material sources derived from Sanyanyu debris flow in Zhouqu County. Northwestern Geology, Vol. 44, No. 3, pp. 21–29 (in Chinese).

Soares-Frazão S.2007, Experiments of dam-break wave over a triangular bottom sill. Journal of Hydraulic Research. Extra Issue Vol. 45, pp. 19–26.

Wang G. Q., Fu X. D., Li T. J., Zhang J. X., Liu F., and Gao J. 2008, Analysis for emergency treatment of quake lakes in Wenchuan earthquake-hit regions. Science of Soil and Water Conservation, Vol. 6, No. 5, pp. 1–6 (in Chinese).

Wu C. and Wu C. G. 1988, Separation of shape-parameters for the calculation of hydraulic characteristics of dam-burst with arbitrary outlet. Shuili Xuebao, No. 9, pp. 10–18 (in Chinese).

Wu C., Zhao W. Q., Zheng Y. H., and Luo L. 1996, A new computational method of dimensionless hydrograph of dam-break with arbitrary outlet. Shuili Xuebao, No. 3, pp. 76–83 (in Chinese).

Yan J. and Cao Z. X. 2009, Experimental study of landslide dam-break flood over erodible bed in open channels. Journal of Hydrodynamics, Ser. B, Vol. 21, No. 1, pp. 124–130.

Yue Z. Y., Cao Z. X., Che T., and Li X. 2007, Two-dimensional mathematical modeling of glacier lake outburst flood. Journal of Glaciology and Geocryology, Vol. 29, No. 5, pp. 756–763 (in Chinese).